# Toward Crack-Free Core–Shell GaN/AlGaN Quantum Wells

Vincent Grenier, Sylvain Finot, Bruno Gayral, Catherine Bougerol, Gwénolé Jacopin, Joël Eymery, Christophe Durand

# Toward crack-free core-shell GaN/AlGaN quantum wells

Vincent Grenier [1,a)], Sylvain Finot[2], Bruno Gayral[1], Catherine Bougerol[2], Gwénolé Jacopin[2], Joël Eymery[3] and Christophe Durand[1]

[1] *Univ. Grenoble Alpes, CEA, IRIG, PHELIQS, NPSC, 38000 Grenoble, France*

[2] *Univ. Grenoble Alpes, CNRS, Grenoble INP, Institut Néel, 38000 Grenoble, France*

[3] *Univ. Grenoble Alpes, CEA, IRIG, MEM, NRS, 38000 Grenoble, France*

a) Author to whom correspondence should be addressed*:* christophe.durand@cea.fr

**Keywords:** Nanowires, MOVPE, GaN/AlGaN MQW, Cracks, Elastic relaxation

## Abstract

Strain relaxation of nonpolar GaN/$Al_{0.6}Ga_{0.4}N$ multiple quantum wells grown in core−shell geometry by metal−organic vapor-phase epitaxy on GaN wire is investigated. Cracking along the *a*-direction is observed on sidewalls of $\bar{c}$-oriented hexagonal GaN wires. To overcome this issue, an undershell including AlGaN gradient and cladding layers are grown before the active region. While a decrease of the crack density is observed with undershell, the increase of GaN QW thickness acts as a key parameter to limit the crack formation. In agreement with previous studies performed on AlGaN planar layers, a relaxation criterion is found for a threshold strain energy density of ~4 J/$m^2$. Considering the quantum well structure as a single AlGaN layer with an average composition, a solution to keep the strain energy density below this relaxation limit is identified by reducing the AlGaN barrier thickness from 5 to 3 nm. Combining undershell and reduced barriers thickness, crack-free core-shell AlGaN-based structure is demonstrated with an emission at 280 nm corresponding to the UV-B/C limit.


## Introduction:

III-nitride ultraviolet (UV) light-emitting diodes (LEDs) are attracting significant interest due to their strengths such as low operating voltages, fast switching capability, compact size, and adjustable wavelengths compared to traditional mercury lamps.[1] For UV-C ($\lambda < 280$ nm) applications, the stakes mainly concern their uses for water and surface sterilization, medical treatment, or gas sensing.[2–4] However, up to now, the state-of-the-art of Al-based UV LEDs reports relatively low EQE values (EQE ≤ 20%) that is attributed to high defect density, poor light extraction and the issue of AlGaN p-doping.[1] Due to the lack of commercially available inexpensive Al(Ga)N bulk substrate, AlGaN-based UV LEDs are mainly grown on sapphire.

However, the large crystal lattice mismatch between sapphire and III-N materials requires buffer layers to grow high-quality materials. GaN, AlGaN, and AlN templates are commonly used as a buffer layer in planar *c*-plane LED architectures depending on the target wavelengths: GaN templates are often integrated for UV-A structures, while AlGaN and AlN templates are employed for UV-B/C emission.[5,6] The main limitations of the GaN template for deep UV emission are UV photon reabsorption and strain accumulation in the Al-rich AlGaN epilayer caused by lattice mismatch (3.5% along *c-axis* and 2.5% along *a-axis* between AlN and GaN). The strain relaxation of this layer generally occurs by crack formation.[7,8] Several solutions to prevent cracks and dislocations in planar structures have been already reported, such as epitaxial lateral overgrowth (ELO) of AlN[9,10] and AlGaN/AlN superlattices.[11] Another strategy is the use of nano/microwire structure to benefit from low intrinsic extended defect density, increased light extraction efficiency and high p-type doping levels achieved in Al-rich AlGaN nanowire materials.[12–15] Focusing on core-shell wires developed by MOVPE, two types of templates corresponding to wire core made of either GaN or AlN have been considered. Similarly to planar structures, GaN wires are generally used to target UV-A,B and AlN wires for UV-C emission.[16,17] In the case of GaN wires, a tunable emission down to 290 nm has been demonstrated with core/shell GaN/AlGaN MQW by decreasing the QW thickness.[18] Moreover, efficient carrier transport as well as electroluminescence in the UV-A,B range have been demonstrated with core-shell AlGaN/GaN n-i-p structures and AlGaN/AlGaN QWs, respectively.[19,20] Although UV-C emission was demonstrated using core-shell AlGaN/AlN QWs on AlN wires, issue of electrical injection into AlN wire impedes the development of electroluminescent (EL) devices. The tuning of the emission wavelength down to UV-B,C emission with a GaN wire as a template remains an issue. Indeed, one of the major challenges stems from the strain relaxation imposed by the wire core on the Al-rich shell required to UV-

B,C emission that leads to crack generation.[21] As the origin of crack formation is directly related to the strain state of the AlGaN/GaN heterostructure, the framework of classical elastic theory is hereafter considered in the case of core-shell structures. Raychaudhuri *et al.* estimate the relative core/shell thicknesses to get a coherent epitaxy from the balance between the elastic strain energy (resulting from lattice mismatch) and the edge dislocation formation energy.[22] This work (confirmed by a more recent publication[23]) points out the existence of a critical core radius, below which the structure is always coherent regardless of shell thickness. On the contrary, structures with core radius exceeding this threshold can still be coherent as long as the shell thickness is below a critical value. As the radius of the core increases, the critical thickness of the shell is approaching the critical thickness of the planar structure. These critical dimensions are obviously not depending on the length of the wire. For the case of GaN core/$Al_xGa_{1-x}N$ shell structures, a critical core radius below 15 nm is reported[22] for an Al-composition larger than 30 %. In the present study, the MOVPE GaN wire diameter will be in the 1-3 µm range. At this scale, statistical measurements showed that there was no correlation between diameter and crack density. Consequently, the core can be considered as quasi-bulk and usual planar elastic calculations describes well the energetics of the epitaxy. The coherent $Al_xGa_{1-x}N$ layer on *m*-GaN template (i.e. GaN wire core) shown in inset of Figure 1a will be considered. The strain components $\varepsilon$ along the *a*- and *c*-axis of the epitaxial layer as a function of Al-content $x$ are defined as following:

$$\varepsilon_a(x) = \frac{a_{Al_xGa_{(1-x)}N} - a_{GaN}}{a_{GaN}} \qquad \varepsilon_c(x) = \frac{c_{Al_xGa_{(1-x)}N} - c_{GaN}}{c_{GaN}} \quad \textbf{(1)}$$

with the respective GaN and $Al_xGa_{(1-x)}N$ lattice parameters *a* and *c*. The *m*-axis strain $\varepsilon_m$ is written as:[24]

$$\varepsilon_m(x) = -\frac{1}{C_{11}}(C_{12}.\varepsilon_a(x) + C_{13}.\varepsilon_c(x)) \quad \textbf{(2)}$$

with the elastic coefficients $C_{11}$, $C_{12}$ and $C_{13}$ of the $Al_xGa_{1-x}N$ alloy considering a linear variation from GaN and AlN binaries (elastic coefficients are given in Table I).[25] Figure 1a shows the respective $\varepsilon_{a,c,m}\ (x)$ strains showing the predominance of $\varepsilon_c\ (x)$, especially for Al-rich AlGaN layer. The elastic energy per volume unit of the deposited layer is written:[24]

$$U_{elastic} = \frac{1}{2}\sum C_{ij}\varepsilon_i\varepsilon_j = \frac{1}{2}(2C_{12}\varepsilon_1\varepsilon_2 + C_{11}(\varepsilon_1^2 + \varepsilon_2^2) + \varepsilon_3(2C_{13}(\varepsilon_1 + \varepsilon_2) + C_{33}\varepsilon_3)) \quad \textbf{(3)}$$

with 1, 2 , 3 corresponding to the *a*, *m* and *c* crystal axes. The elastic energy per surface unit is calculated in Figure 1b for different layer thicknesses *h* ranging from 5 to 100 nm as a function of *x,* the composition of the strained $Al_xGa_{1-x}N$ layer. In this ideal case, the elastic energy per surface unit linearly increases with the layer thickness *h* and has a quadratic dependence on *x*. It can be also shown that the strain associated to the thermal expansion coefficients of GaN and AlN does not contribute to the elastic relaxation studied in this work (see supporting information S1).

| | *a (Å)* | *C (Å)* | $C_{11}$ (GPa) | $C_{12}$ (GPa) | $C_{13}$ (GPa) | $C_{33}$ (GPa) | $\alpha_a$ | $\alpha_c$ | $\theta_a$ | $\theta_c$ |
|---|---|---|---|---|---|---|---|---|---|---|
| **GaN** | 3.189 | 5.185 | 367 | 135 | 103 | 405 | $6.2*10^{-6}$ | $5.7*10^{-6}$ | 636 | 662 |
| **AlN** | 3.112 | 4.982 | 396 | 137 | 108 | 373 | $6.9*10^{-6}$ | $5.6*10^{-6}$ | 1025 | 937 |

*Table 1 : Lattice parameters, elastic coefficients[25] and thermal expansion coefficients[26] of the GaN and AlN bulk materials used in this study.*

This study focused on GaN/AlGaN core-shell wire heterostructures aims to limit and even to suppress the crack formation by managing the strain relaxation while targeting emission in the UV-A,B range. A systematic study of the crack density along wires carried out to determine the predominant factors involved in the crack formation in a core-shell system. In this approach, the influence of underlayers preceding the MQWs is studied by comparing two

different types of shells and the impact of the GaN QW and AlGaN barrier thicknesses on crack formation is investigated.

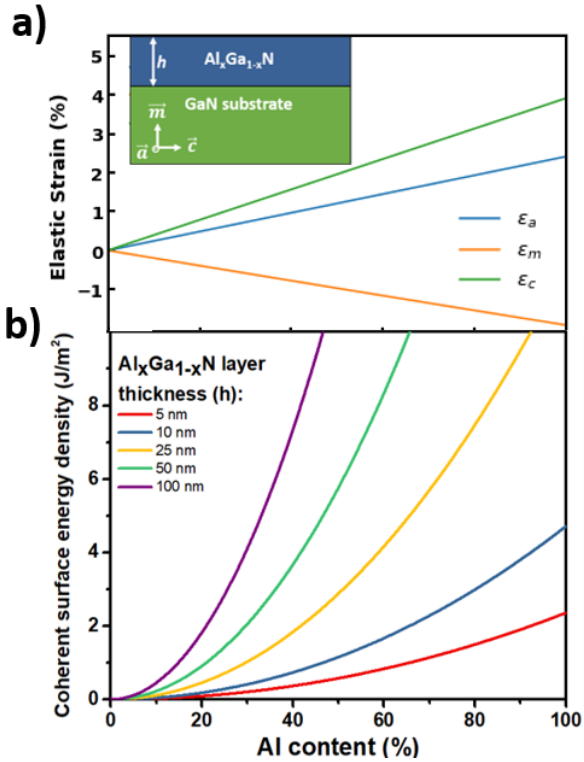


*Figure 1 : a) Elastic strain along the c, a and m axes as a function of the Al content for a coherent 2D layer of $Al_xGa_{1-x}N$ on GaN substrate (see inset). b) Corresponding elastic energy density per unit area for several thicknesses h of the $Al_xGa_{1-x}N$ layer.*

## Experimental part:

The growth of self-assembled GaN microwires on *c*-sapphire is performed in a close coupled showerhead MOVPE reactor with the silane-assisted method and small V/III ratio described in reference.[27] The sapphire substrate is first annealed at 1050°C under $NH_3$ to get an Al-terminated surface that will promote the growth of N-polar wires. The surface preparation goes on by the simultaneous injection of silane ($SiH_4$) and ammonia ($NH_3$) to form a very thin $SiN_x$ layer, known to be a selective layer for the growth of GaN. The epitaxial growth nucleation occurring through this layer is obtained by the injection of trimethylgallium (TMGa) (135 µmol.min$^{-1}$) and $NH_3$ (2.23 mmol.min$^{-1}$) (i.e. very low V/III ratio ~50) diluted in $N_2$ carrier gas

flow (8000 sccm) at 1040°C and 800 mbar. After 10 s, a high flux of silane is added (~200 nmol.min$^{-1}$) to form a thin $SiN_x$ passivation layer on the *m*-plane sidewalls of the GaN wires. This selective layer does not grow on the upper $\bar{c}$-plane, promoting the vertical growth of the wires.[27] Note also that such a high flux of silane leads to a heavily doped GaN (called $n^{++}$, $N_d$ ~ $10^{20}$ cm$^{-3}$), which eases current injection in wire devices.[28] Silane is switched off after 300 s, and the V-III flow is maintained for 400 s. During this time, the silane remaining in the reactor allows the GaN wire growth going on, but with a smaller residual doping (called $n^{+}$, $N_d$ ~ $10^{19}$ cm$^{-3}$).[29] The two $n^{++}$ and $n^{+}$ doped GaN regions therefore correspond to the lower and upper part of the wire, respectively. During the entire wire growth, the temperature is maintained at 1040°C. Then, a 50 nm-thick GaN shell (referred to as "GaN spacer" hereafter) is grown at 900°C and 150 mbar using $NH_3$ and TMGa fluxes of 66.9 mmol.min$^{-1}$ and 24.8 µmol.min$^{-1}$, respectively (~2700 V/III ratio). This GaN spacer growth occurs only on $SiN_x$-free zone (i.e. at the upper part of the wire) and allows burying the surface defects induced by the residual silane.[30,31] To prepare the growth conditions for the MQWs, the Ga source is shifted to triethylgallium (TEGa) for 10 min (3.6 µmol.min$^{-1}$ molar flux and ~18000 V/III ratio). The same growth parameters are maintained to grow GaN/AlGaN MQWs except the pressure that is decreased to 100 mbar to prevent trimethylaluminium (TMAl) pre-reactions in the gas phase. The barriers of the MQWs are grown using 3.6 µmol.min$^{-1}$ TEGa and 7.3 µmol.min$^{-1}$ TMAl flows (i.e. ~18000 and ~6000 V/III ratios for QWs and barriers). These growth conditions lead to ~60 % of Al-content as measured in reference [18].

In this work, two kinds of shells are studied with 5x(GaN/$Al_{0.6}Ga_{0.4}N$) MQWs grown directly on the GaN wires (called “structure A”) and after the insertion of an AlGaN linear gradient from 0 to 30% Al and a 20 nm-thick $Al_{0.3}Ga_{0.7}N$ layer (called “structure B”). In this case, under the same pressure (100 mbar) and temperature (900 °C) as the rest of the shell, the gradient is

grown for 1000 s to target ~50 nm thickness. Combined to a continuous TEGa flux of 3.6 µmol.min$^{-1}$, the TMAl flux varies linearly from 0 to 3.7 µmol.min$^{-1}$ to obtain a maximum Al-composition of ~30 %. For the cladding layer, the growth duration is 600 s with a constant TMAl flux of 3.7 µmol.min$^{-1}$. Finally, the TEGa flux is kept constant at 3.6 µmol.min$^{-1}$ to growth the A and B shell heterostructures. The QW growth time is varied (120, 60, 20, and 10 s) to reduce the QW thickness, whereas the $Al_{0.6}Ga_{0.4}N$ barrier growth time is either 70 s to get 5 nm thickness or 45 s for 3 nm. To encapsulate the last AlGaN layer, a thin GaN cap of 1.5-2.5 nm is grown using similar conditions to the GaN spacer.

## Discussion:

Regarding to the A-type, B-type core shell structure have been designed to target an efficient optical emission in UV-A,B by managing the strain relaxation process : i.e., by obtaining a relaxed layer with a smaller parameter than the GaN core convenient for the active emission structure. To favor relaxation, we propose here to use a $Al_xGa_{1-x}N$ gradient promoting dislocation interactions and annihilations. Their schematics is shown in Figure 2a,b. As an example, Figure 2c and d show scanning electron microscopy (SEM) images of the upper part of representative A and B core-shell GaN wires with similar MQW heterostructures (i.e., 5 GaN QWs grown in 20 s separated by 5 nm $Al_{0.6}Ga_{0.4}N$ barriers). They reveal the presence of micrometer-sized cracks indicated by white arrows. These cracks are mostly perpendicular to the *c*-axis and progress along the *a*-crystallographic direction of the wire lateral surfaces. Some cracks are slightly inclined toward up or down direction, which can be attributed to additional strain relaxation along a-axis ($\varepsilon_a$) by the formation of kinks along the c direction, due to the biaxial anisotropy stress of the m-plane surface (see Figure 1a). The bifurcation of the crack line propagation will depend on the local strain, but also on the spatial coupling that can

explain bunches of orientation along the wires. Note also that the kinetics of the crack set has to be considered: local nucleation of individual cracks do not occur at the same time and strain relaxation dynamics should be taken into account to explain the complete process.[32,33]

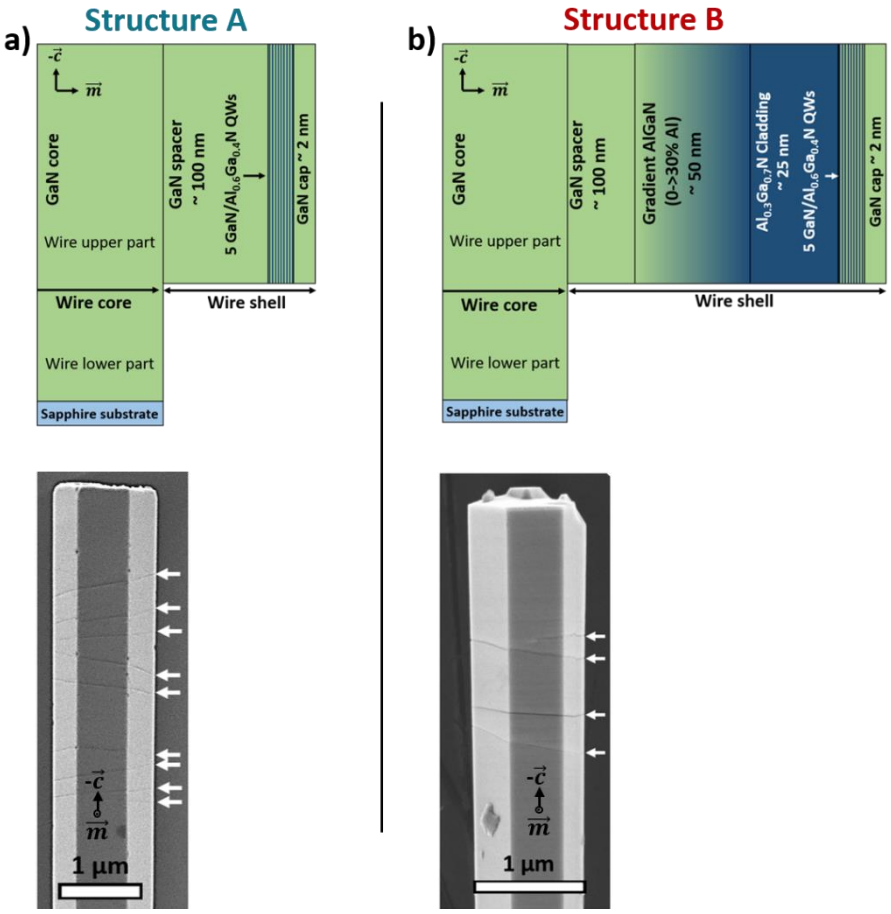


*Figure 2: Schematics and side view SEM images of the upper part of a) A-type wire shell composed of GaN spacer and 5x(0.43 nm GaN/ 5 nm $Al_{0.6}Ga_{0.4}N$) multiple quantum well capped by a few nanometers of GaN. b) B-type wire with 50 nm AlGaN gradient (varying linearly the Al composition from 0 to ~30%) and a 20 nm cladding layer of $Al_{0.3}Ga_{0.7}N$ added to the structure A between the GaN spacer and the heterostructure. The 0.43 nm of the GaN wells correspond to 20 s growth time. The presence of cracks is indicated by white arrows.*

For both structures A and B, a first series of samples is studied by varying the QW thickness with the growth time. Based on TEM measurements previously performed on these structures,[18] the QW and barrier growth rates have been measured to be equal to $V_{QW}$ = 1.3 ± 0.5 nm.min$^{-1}$ and $V_{barrier}$ = 4.3 ± 1.2 nm.min$^{-1}$, and the estimated thicknesses are therefore 5 nm for the barriers and from 2.6 to 0.2 nm for GaN QW (for growth time varying from 120 to

10 s). As an example, Figure 3a shows some SEM images of the upper part of A-type core-shell GaN wires for several GaN QW growth times (120, 60, 20, 10 s). It reveals the presence of micrometer-size cracks (indicated by white arrows) increasing in density for thinner QW samples. This tendency is confirmed in Figure 3b by the measurement of the linear density of cracks as a function of the GaN QW thickness (statistics made on 50 wires, see supporting information S3). It shows that the reduction of QW thickness from 2.6 to 0.2 nm leads to a significant increase of the crack linear density from ~0 to 1.3 $\mu m^{-1}$ for the structure A and from ~0 to 0.7 $\mu m^{-1}$ for the structure B. It is interesting to note that the structure B having an additional interlayer of AlGaN compared to structure A has a lower density of cracks for the same QW thickness. The AlGaN gradient with cladding layer probably adds a new pathway to relax the epitaxial strain and therefore delays the micro-crack formation.[34] .The structural characterization by TEM performed on a wire containing an AlGaN gradient without cladding layer does not show other defects such as dislocations in the gradient layer and in the MQW structure (see Fig. S2 in the Supporting Information). In addition, we note that the cracks propagate beyond the wire core.

As reported by Einfeldt *et al*.,[8,32] the formation of micro-cracks along the *a*-direction is usual in $Al_xGa_{1-x}N$ layers grown on GaN/sapphire substrates. It occurs if the Al content exceeds a critical value, which decreases with increasing layer thickness. As demonstrated by X-ray measurements, the crack process occurs when the average strain energy density reaches a value beyond ~4 $J/m^2$. Using the expression of $U_{elastic}$ from equation (3) and the elastic surface energy threshold value of 4 $J/m^2$, the critical thickness for a *m*-plane AlGaN layer depending on aluminum composition can be calculated and results are reported in Figure 4a with a black dashed line and squares. In this figure, no crack should be formed in the region below this line.

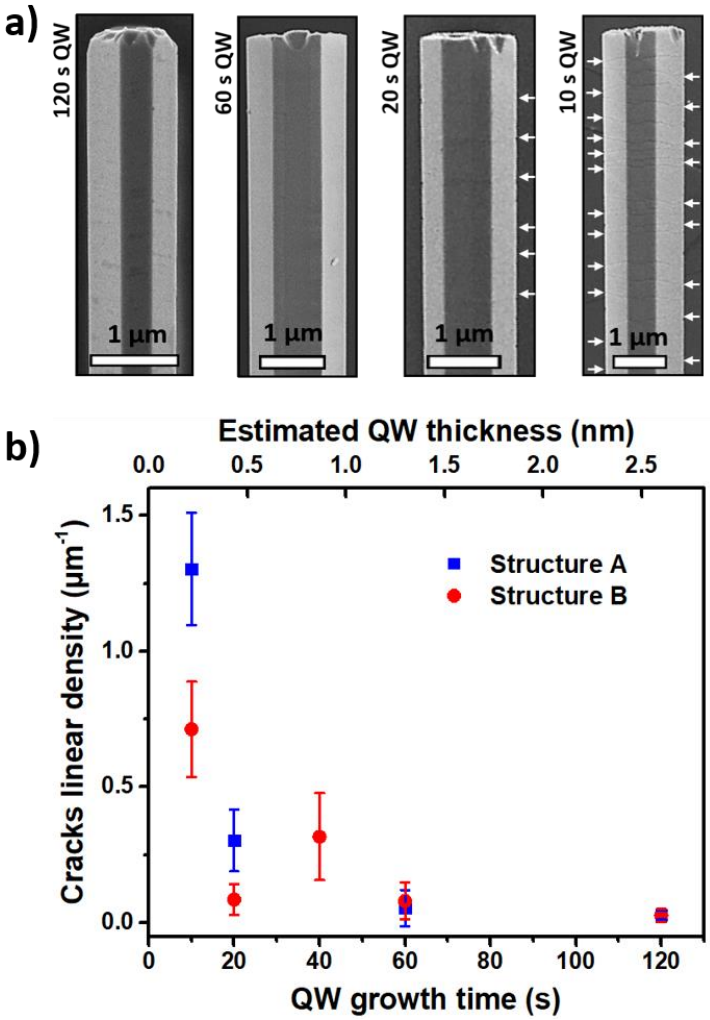


*Figure 3: a) Top view SEM image of the upper part of a A-type wire with QW thicknesses changing from 2.6 to 0.2 nm (the growth time being varied from 120 to 10 s). The presence of cracks is indicated by white arrows. b) Measured linear density of cracks as a function of the GaN QW thickness for both A- and B-type wires. For each sample, 50 wires are considered and error bar corresponds to 95% deviation from the mean value.*

In order to simplify the calculations for the core-shell 5x MQW heterostructures, we consider an equivalent AlGaN single layer of total thickness:

$$L_{\mathrm{AlGaN}} = 6 * L_{\mathrm{barrier}} + 5 * L_{\mathrm{QW}} \quad \textbf{(4)}$$

where $L_{\mathrm{barrier}}$ and $L_{\mathrm{QW}}$ are respectively the barrier and QW thicknesses and, to mimic a strain-balanced configuration, we assume that the in-plane lattice parameter of the

equivalent single layer corresponds to the $Al_{\bar{x}}Ga_{1-\bar{x}}N$ ternary alloy with the average Al composition $\bar{x}_{\mathrm{Al}}$ of the MQW period:

$$\bar{x}_{\mathrm{Al}} = (6 * L_{\mathrm{barrier}} * X_{\mathrm{barrier}})/L_{\mathrm{AlGaN}} \quad \textbf{(5)}$$

with $X_{\mathrm{barrier}}$ the barriers composition (60% in this study).[18] Thus, for each A-type samples with different GaN QW thickness, the heterostructures is considered as a single AlGaN layer described by the total thickness $L_{\mathrm{AlGaN}}$ and the average aluminum composition $\bar{x}_{\mathrm{Al}}$ (corresponding values are given in Table 2).

Figure 4a shows the calculated values of the critical thickness for an average Al-value $\bar{x}$ for two $L_{\mathrm{barrier}}$ values: 5 nm (blue line) and 3 nm (red line) and for several QW growth times (10, 20, 60 and 120 s). This calculation is consistent with the crack appearance occurring in type-A samples for QW growth time less than 60 s (see Figure 3b) and validates that the elastic density criteria threshold (4 J/m$^2$) can be also considered for *m*-plane growth. The same model predicts that a barrier thickness reduction from 5 nm to 3 nm should overcome the crack formation (see the red line/symbols in Figure 4a). In order to validate this prediction, two new A-type samples were grown with 3 nm-thick barrier and QW growth time of 20 and 10 s corresponding to 0.43 and 0.22 nm thickness, respectively. The SEM comparison of 10 s QW growth time (i.e., the most unfavorable case in terms of energy value) with 5 and 3 nm barriers is shown in Figure 4b. As predicted by the elastic calculation model, the sample grown with 3 nm-thick barriers does not exhibit any cracks, whereas the cracks clearly occur for the 5 nm-thick barrier sample with a linear crack density larger than 1.3 cracks per µm. The measurements of the linear crack density as a function of the surface elastic energy calculated for the corresponding single $Al_{\bar{x}}Ga_{1-\bar{x}}N$ layer model shown in Figure 4c endorses the relevance of the energetic threshold criteria. In this figure, a very low linear crack density is

demonstrated for samples with elastic energy per unit area below the threshold value of 4 J/m$^2$ as expected from the observations of *c*-planar AlGaN films by Einfeldt *et al*.

| QW growth time (s) | $L_{barrier}$ (nm) | $\overline{x}_{Al}$ (%) | $L_{AlGaN}$ (nm) |
|---|---|---|---|
| 120 | 5 | 42 | 43 |
| 60 | 5 | 49 | 36.5 |
| 20 | 5 | 56 | 32.15 |
| 10 | 5 | 58 | 31.05 |
| 120 | 3 | 35 | 31 |
| 60 | 3 | 44 | 24.5 |
| 20 | 3 | 54 | 20.15 |
| 10 | 3 | 57 | 19.05 |

*Table 2 : Calculated Al content and thickness of the equivalent single $Al_{\bar{x}}Ga_{1-\bar{x}}N$ layer for several QW growth time and barrier thickness.*

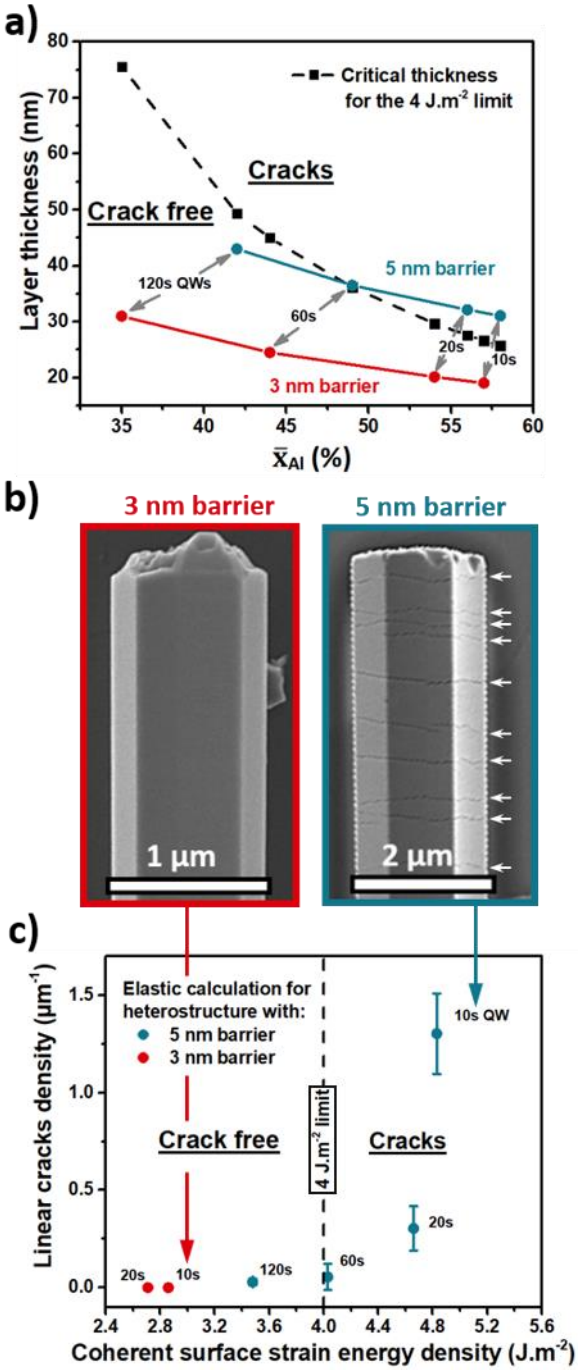


*Figure 4: a) Calculated critical thickness of an AlGaN layer on m-plane GaN as a function of the Al-content $\bar{x}$ (black line and symbols). Calculations for A-type wires considering an equivalent AlGaN single layer of mean Al-value $\bar{x}$ for different QWs growth times (120 to 10 s) and for two barrier thicknesses: 5 nm (blue line) and 3 nm (red line). b) Top-view SEM images of the upper part of an A-type wire with 10 s QWs growth time and for the two $Al_{0.6}Ga_{0.4}N$ barrier thicknesses. Cracks are indicated by white arrows. c) Linear crack density as a function of the surface elastic energy calculated for a single $Al_{\bar{x}}Ga_{1-\bar{x}}N$ layer having QW growth times varying from 120 to 10 s and the two barrier thicknesses (5 nm, blue dots and 3 nm, red dots). The experimental elastic density threshold (4 J/m$^2$) determined in Reference [8] is indicated by a vertical dotted line.*

Cathodoluminescence (CL) experiments are carried out to investigate the optical properties of the wires, especially the impact of the cracks on the emission. Measurements are performed with a field emission (FEG)-SEM (working at 5 kV acceleration voltage and 1 nA current) equipped with a helium cryostat. The CL signal is collected by a parabolic mirror and analyzed by a monochromator coupled to a charge-coupled device detector. Wires are dispersed on silicon substrates by mechanical scratching. A brittle fracture is favored by dislocations generated at the sapphire/wire interface. This operation is required to prevent light emission from any residual growth on the sapphire substrate. Figure 5a shows a SEM image of a typical wire without cracks (A-type structure with 5 nm $Al_{0.6}Ga_{0.4}N$ barriers and large GaN QW thickness corresponding to a growth time of 200 s) and its CL intensity map measured at low temperature (~5 K). The CL intensity signal integrated over a range of wavelengths from 309 to 380 nm shows the optical emission that corresponds to the MQW shell and the GaN core of the upper part of a typical wire. Figure 5b shows a SEM image of a typical cracked wire (also A-type structure but with 5 nm $Al_{0.6}Ga_{0.4}N$ barriers and thin GaN QW thickness corresponding to a growth time of 20 s) and a CL intensity maps at ~5 K: intensity integration over the 270-328 nm range corresponds to the GaN/AlGaN MQW emission. The whole emission is quenched at the crack locations, probably due a local decrease of the efficiency as observed by Finot *et al*.[21] on core-shell AlGaN/AlGaN MQWs. In our study, the CL signal comes from the regions between the cracks, showing a strong influence of these extended defects on the QW emission.

Photoluminescence (PL) experiments are additionally carried out on dispersed wires using a continuous-wave frequency-doubled solid-state laser at 244 nm wavelength and a spot diameter around 50 µm, the measurements are performed using a 1 mW excitation power leading to about 50 $W.cm^{-2}$ power density. Figure 5c presents the normalized PL spectra

measured at 5 K for four samples having similar QW thickness estimated at 0.43 nm with A- and B-structures and 3 and 5 nm-thick barriers. It is found that the B-type structure leads to a systematic blue shift of the QW emission and to a reduction of the full width at half maximum (FWHM) with respect to the A-type. For both structures, we also notice a FWHM variation between samples with 5 and 3 nm barriers. Consistent with the crack erasing, the use of thinner barriers leads to a FWHM reduction from 320 to 280 meV for the A-type and from 250 to 225 meV for the B-type structure. Considering the above results, the use of structure B combined with reduced barrier thicknesses provides crack-free core-shell wires with reduced FWHM and a deeper UV emission.

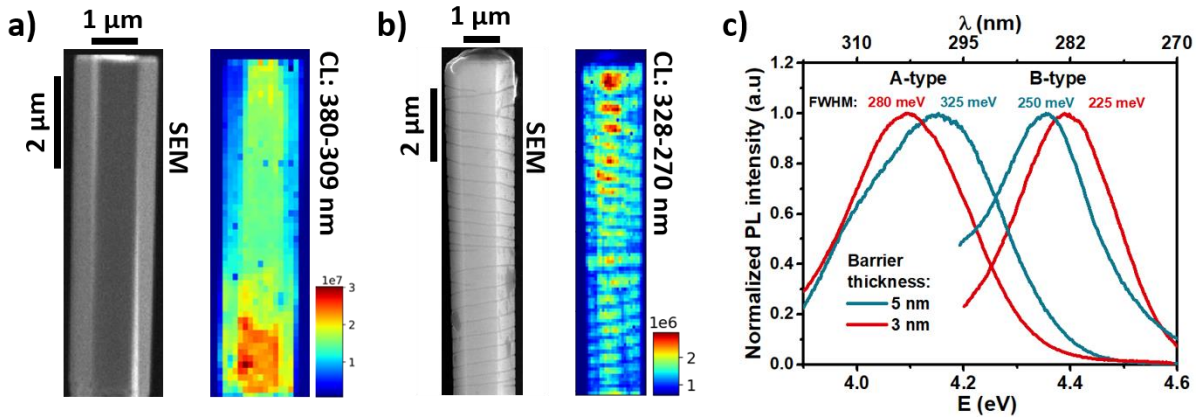


*Figure 5: (a, b) SEM image of a typical single A-type wire and its corresponding CL mapping performed at 5 K. a) Wires grown with GaN QWs for 200 s do not present any crack. b) Wires grown with GaN QWs for 20 s present many cracks that impact the CL mapping. c) Normalized PL spectra at 5 K of the QW emission for four samples with 20 s QW growth time for both A- and B-type samples, and 5 and 3 nm $Al_{0.6}Ga_{0.4}N$ barriers. An assembly of wires are dispersed on silicon (laser at 244 nm wavelength and an excitation power ~50 $W{\cdot}cm^{-2}$).*

A general overview of the optical characterization of the samples is provided in Figure 6 plotting the PL energy emission of the GaN QWs as a function of their estimated thicknesses. Horizontal error bars are calculated by considering an error of 20% on the estimated nominal GaN QW thickness and the vertical error bars correspond to the dispersion of the PL energy for the measurements acquired at four positions of the assemblies under the same excitation

conditions. The evolution of the PL emission energy as a function of the QW thickness is basically consistent with the absence of quantum-confined Stark effect (QCSE) in nonpolar *m*-plane MQWs. Indeed, increasing the QW thickness leads to a monotonous decrease of the emission energy to reach the expected asymptotical value of the bulk GaN bandgap, as previously reported in GaN/AlGaN[36] and GaN/InAlN core-shell MQWs.[24] In this figure, the experimental data are compared to the calculations (colored dashed lines) performed with the nextnano3 software[37] using the 8-band k·p Schrödinger–Poisson method (see parameter values in reference [36]). Lattice parameters and elastic coefficients of ternary alloys are extracted from those of binary compounds (given in Table 1) by linear interpolation. We modeled five periods of GaN/$Al_{0.6}Ga_{0.4}N$ MQWs with 5 nm thick barriers with a one-dimensional description. To estimate the influence of the strain on the optical emission of MQWs, two cases have been considered. We calculate the emission for a pseudomorphic growth on GaN (i.e., $Al_{0.6}Ga_{0.4}N$ is fully strained, green dashed line) and on $Al_{0.6}Ga_{0.4}N$ (i.e., GaN is fully strained, yellow dashed line). The systematic increase in the emission energy of structure B compared to structure A is interpreted as an effect of the QW strain. Indeed, as observed in Figure 3b, structure B shows a reduction of the crack density, suggesting that the AlGaN gradient layer provides a partial relaxation of the strain leading to a higher strain state for the GaN QWs. Another observation concerns the saturation of the emission energy for both A- and B-type samples with estimated QW thicknesses less than 0.5 nm. We suspect that the growth conditions used in this study do not favor very thin QWs of few monolayers (ML), but rather the formation of quantum dots, as observed on the TEM characterization (see Figure S2 of supporting Information).

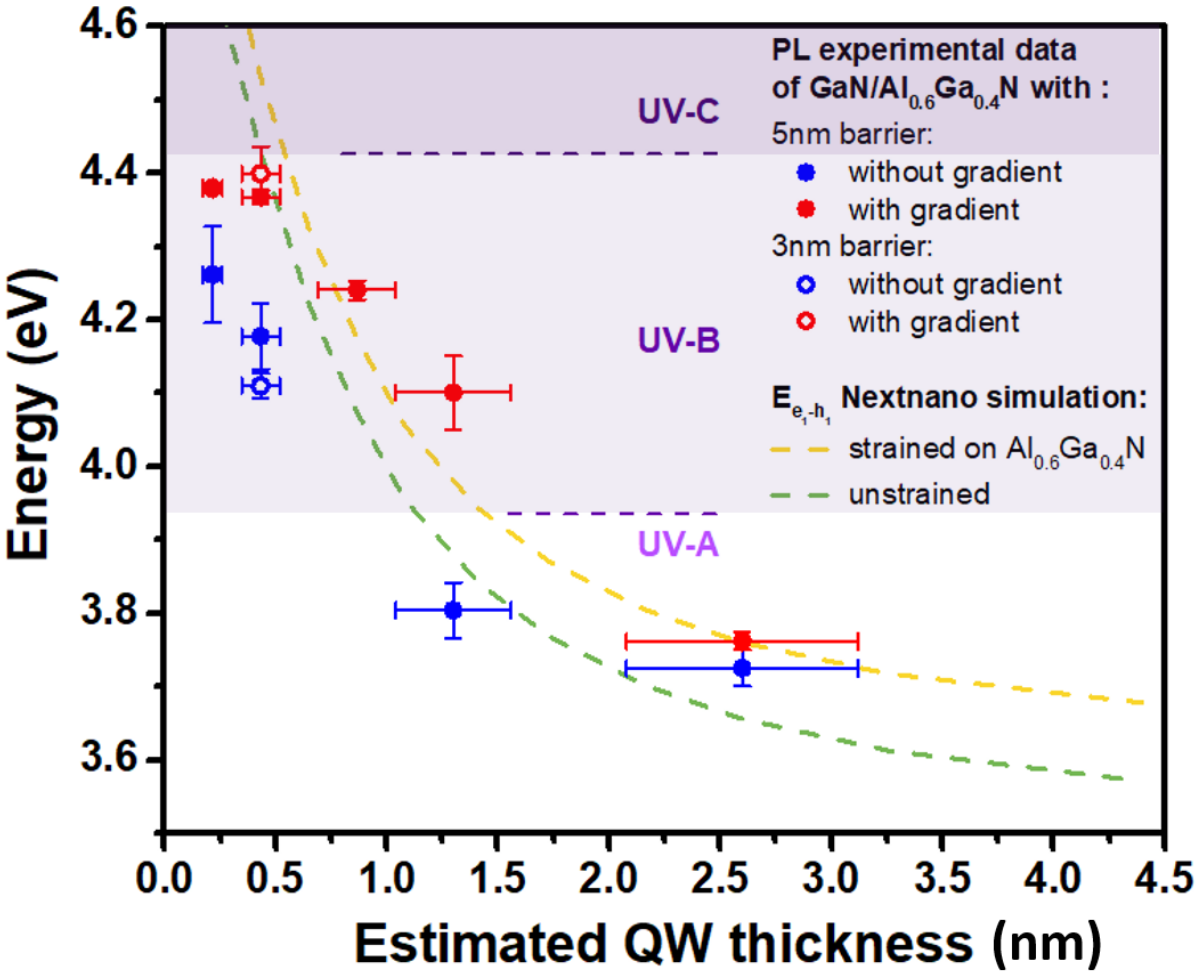


*Figure 6: PL emission energy of GaN QWs as a function of their estimated thickness for A-type (blue dots) and B-type (red dots) samples (see description in Figure 2). Measurements are performed at 5 K on wire assemblies dispersed on silicon. Laser wavelength is 244 nm, and excitation power is* about *50 W·cm$^{-2}$. Samples with 5 and 3 nm $Al_{0.6}Ga_{0.4}N$ barriers are represented by full and open circles, respectively. Experimental data are compared to nextnano3 calculations (colored dashed lines) of the GaN QWs emission in two limit cases of strain states:* GaN QWs fully strained *to $Al_{0.6}Ga_{0.4}N$ (yellow line) and fully relaxed (green line).*

## Conclusion:

This paper reports the crack formation generated by core-shell GaN/$Al_{0.6}Ga_{0.4}N$ MQWs on GaN microwires grown by MOVPE. The presence of microcracks propagating perpendicular to the $\bar{c}$-axis is consistent with elastic calculations considering wire core as quasi-bulk substrate, as similarly observed in *c*-planar structures. An undershell has been designed by implementing AlGaN gradient and $Al_{0.3}Ga_{0.7}N$ cladding layers grown before the GaN/$Al_{0.6}Ga_{0.4}N$ MQW

structure in order to favor a progressive strain relaxation by activating other mechanisms than crack formation (dislocation generation and interactions). While the AlGaN undershell effect is limited, the QW thickness strongly impacts the crack formation. The key-point to achieve crack-free core-shell structures is related to the critical elastic energy per surface unit as previously demonstrated in c-planar growths, empirically estimated about 4 J/m$^2$. According to this limit, a complete vanishing of cracks is achieved when the AlGaN barrier thickness is reduced from 5 to 3 nm. The crack-free wires exhibit improved optical properties, since the QW emission is quenched around the cracks. The presence of AlGaN undershell favors a systematic UV-shift of the QW emission. Emission as low as 4.4 eV (280 nm) corresponding to the UV-B/C limit is achieved for thinner QWs. This demonstration of crack-free core-shell AlGaN-based structure is a step forward towards wire-LED devices emitting in the UV-C range.

## Supporting information:

The Supporting Information is available free of charge at XXX.
Calculation of the thermal expansion strain of an $Al_{0.6}Ga_{0.4}N$ layer on a *m*-plane GaN substrate; Structural characterization of a core-shell wire by scanning transmission electron microscopy (STEM) with the high-angle annular dark field (HAADF) method; The measurement statistics of the linear density of the cracks.

## Author information

**Corresponding Authors**
**Vincent Grenier** − *Université Grenoble Alpes*, CEA, IRIG, PHELIQS, NPSC, 38000 Grenoble, France; orcid.org/0000-0003-2781-0559; Email: vincent.grenier@cea.fr
**Christophe Durand** − *Université Grenoble Alpes*, CEA, IRIG, PHELIQS, NPSC, 38000 Grenoble, France; orcid.org/ 0000-0002-5012-8411; Email: christophe.durand@cea.fr

**Authors**
**Sylvain Finot** − *Université Grenoble Alpes*, CNRS, Grenoble INP, Institut Néel, 38000 Grenoble, France; orcid.org/0000-0003-1455-7160

**Gwénolé Jacopin** − *Université Grenoble Alpes*, CNRS, Grenoble INP, Institut Néel, 38000 Grenoble, France; orcid.org/0000-0003-0049-7195
**Catherine Bougerol** − *Université Grenoble Alpes*, CNRS, Grenoble INP, Institut Néel, 38000 Grenoble, France; orcid.org/0000-0002-4823-0919
**Bruno Gayral** − *Université Grenoble Alpes*, CEA, IRIG, PHELIQS, NPSC, 38000 Grenoble, France; orcid.org/0000-0002-3724-1380
**Joël Eymery** − *Université Grenoble Alpes*, CEA, IRIG, MEM, NRS, 38000 Grenoble, France; orcid.org/0000-0002-4216-1166

## Author Contributions

V.G. performed the wire growth process and took an active part in the writing of this manuscript with support from the supervisors C.D. and J.E. who designed the study. S.F and G.J performed the cathodoluminescence measurements and data treatments. C.B. performed the STEM/TEM measurements. The FIB preparation, photoluminescence measurements (thanks to the trainings B.G), and nextnano3 calculations were performed by V.G. All authors contributed to the discussions and have given approval to the final version of the manuscript. The authors declare no competing financial interest.

## Acknowledgements:

This work was financially supported by the program Initiatives de Recherche Stratégiques (IRS) of IDEX Université Grenoble Alpes (15-IDEX-0002) and by the French ANR-19-CE42-0016 PiezoSens. The authors warmly thank J. Dussaud for his decisive help on the MOVPE setup.

## References

(1) Kneissl, M.; Seong, T. Y.; Han, J.; Amano, H. The Emergence and Prospects of Deep-Ultraviolet Light-Emitting Diode Technologies. *Nature Photonics*. 2019, 233–244.

(2) Shur, M.; Shatalov, M.; Dobrinsky, A.; Gaska, R. Deep Ultraviolet Light-Emitting Diodes. *Springer Series in Materials Science*. 2012, *Vol. 156*, 83–120.

(3) Mehnke, F.; Guttmann, M.; Enslin, J.; Kuhn, C.; Reich, C.; Jordan, J.; Kapanke, S.; Knauer, A.; Lapeyrade, M.; Zeimer, U.; et al. Gas Sensing of Nitrogen Oxide Utilizing Spectrally Pure Deep UV LEDs. *IEEE.* 2017, *Vol. 23*, 29–36.

(4) Buonanno, M.; Ponnaiya, B.; Welch, D.; Stanislauskas, M.; Randers-Pehrson, G.;

Smilenov, L.; Lowy, F. D.; Owens, D. M.; Brenner, D. J. Germicidal Efficacy and Mammalian Skin Safety of 222-nm UV Light. *Radiat. Res.* 2017,*Vol. 187*, 483–491.

(5) Yan, J.; Wang, J.; Zhang, Y.; Cong, P.; Sun, L.; Tian, Y.; Zhao, C.; Li, J. AlGaN-Based Deep-Ultraviolet Light-Emitting Diodes Grown on High-Quality AlN Template Using MOVPE. *J. Cryst. Growth.* 2015,*Vol. 414*, 254–257.

(6) Khan, M. A.; Maeda, N.; Jo, M.; Akamatsu, Y.; Tanabe, R.; Yamada, Y.; Hirayama, H. 13 MW Operation of a 295-310 nm AlGaN UV-B LED with a p-AlGaN Transparent Contact Layer for Real World Applications. *J. Mater. Chem. C.* 2019, *Vol. 7*, 143–152.

(7) Itoh, K.; Hiramatsu, K.; Amano, H.; Akasaki, I. PREPARATION OF AlxGa(1-x)N/GaN HETEROSTRUCTURE BY MOVPE. *J. Cryst. Growth.* 1990, *Vol. 104*, 533–538.

(8) Einfeldt, S.; Kirchner, V.; Heinke, H.; Dießelberg, M.; Figge, S.; Vogeler, K.; Hommel, D. Strain Relaxation in AlGaN under Tensile Plane Stress. *J. Appl. Phys.* 2000, *Vol. 88*, 7029–7036.

(9) Imura, M.; Nakano, K.; Narita, G.; Fujimoto, N.; Okada, N.; Balakrishnan, K.; Iwaya, M.; Kamiyama, S.; Amano, H.; Akasaki, I.; *et al*. Epitaxial Lateral Overgrowth of AlN on Trench-Patterned AlN Layers. *J. Cryst. Growth.* 2007, *Vol. 298*, 257–260.

(10) Zeimer, U.; Kueller, V.; Knauer, A.; Mogilatenko, A.; Weyers, M.; Kneissl, M. High Quality AlGaN Grown on ELO AlN/Sapphire Templates. *J. Cryst. Growth.* 2013, *Vol. 377*, 32–36.

(11) Kim, J.; Pyeon, J.; Jeon, M.; Nam, O. Growth and Characterization of High Quality AlN Using Combined Structure of Low Temperature Buffer and Superlattices for Applications in the Deep Ultraviolet. *Jpn. J. Appl. Phys.* 2015, *Vol. 54*. 081001

(12) Connie, A. T.; Zhao, S.; Sadaf, S. M.; Shih, I.; Mi, Z.; Du, X.; Lin, J.; Jiang, H. Optical and Electrical Properties of Mg-Doped AlN Nanowires Grown by Molecular Beam Epitaxy.

*Appl. Phys. Lett.* 2015, *Vol. 106*, 213105.

(13) Tran, N. H.; Le, B. H.; Zhao, S.; Mi, Z. On the Mechanism of Highly Efficient P-Type Conduction of Mg-Doped Ultra-Wide-Bandgap AlN Nanostructures. *Appl. Phys. Lett.* 2017, *Vol. 110*, 032102.

(14) Siladie, A. M.; Jacopin, G.; Cros, A.; Garro, N.; Robin, E.; Caliste, D.; Pochet, P.; Donatini, F.; Pernot, J.; Daudin, B. Mg and in Codoped P-Type AlN Nanowires for Pn Junction Realization. *Nano Lett.* 2019, *Vol. 19*, 8357–8364.

(15) Laleyan, D. A.; Zhao, S.; Woo, S. Y.; Tran, H. N.; Le, H. B.; Szkopek, T.; Guo, H.; Botton, G. A.; Mi, Z. AlN/h-BN Heterostructures for Mg Dopant-Free Deep Ultraviolet Photonics. *Nano Lett.* 2017, *Vol. 17*, 3738–3743.

(16) Coulon, P. M.; Kusch, G.; Martin, R. W.; Shields, P. A. Deep UV Emission from Highly Ordered AlGaN/AlN Core-Shell Nanorods. *ACS Appl. Mater. Interfaces.* 2018, *Vol. 10*, 33441–33449.

(17) Kim, J.; Choi, U.; Pyeon, J.; So, B.; Nam, O. Deep-Ultraviolet AlGaN/AlN Core-Shell Multiple Quantum Wells on AlN Nanorods via Lithography-Free Method. *Sci. Rep.* 2018, *Vol. 8*, 935.

(18) Grenier, V.; Finot, S.; Jacopin, G.; Bougerol, C.; Robin, E.; Mollard, N.; Gayral, B.; Monroy, E.; Eymery, J.; Durand, C. UV Emission from GaN Wires with M-Plane Core-Shell GaN/AlGaN Multiple Quantum Wells. *ACS Appl. Mater. Interfaces.* 2020, *Vol. 12, 44007−44016*.

(19) Brubaker, M. D.; Genter, K. L.; Roshko, A.; Blanchard, P. T.; Spann, B. T.; Harvey, T. E.; Bertness, K. A. UV LEDs Based on P-i-n Core-Shell AlGaN/GaN Nanowire Heterostructures Grown by N-Polar Selective Area Epitaxy. *Nanotechnology.* 2019, *Vol. 30*, 234001.

(20) Ra, Y. H.; Kang, S.; Lee, C. R. Ultraviolet Light-Emitting Diode Using Nonpolar AlGaN Core–Shell Nanowire Heterostructures. *Adv. Opt. Mater.* 2018, *Vol. 6*, 1701391.

(21) Finot, S.; Grenier, V.; Zubialevich, V.; Bougerol, C.; Pampili, P.; Eymery, J.; Parbrook, P. J.; Durand, C.; Jacopin, G. Carrier Dynamics near a Crack in GaN Microwires with AlGaN Multiple Quantum Wells. *Appl. Phys. Lett.* 2020, *Vol. 117*, 221105.

(22) Raychaudhuri, S.; Yu, E. T. Calculation of Critical Dimensions for Wurtzite and Cubic Zinc Blende Coaxial Nanowire Heterostructures. *J. Appl. Phys.* 2006, *Vol. 99*, 114308.

(23) Ferrand, D.; Cibert, J. Strain in Crystalline Core-Shell Nanowires. *Eur. Phys. J. Appl. Phys*. 2014, *Vol.* 67, 30403

(24) Durand, C.; Bougerol, C.; Carlin, J. F.; Rossbach, G.; Godel, F.; Eymery, J.; Jouneau, P. H.; Mukhtarova, A.; Butté, R.; Grandjean, N. M-Plane GaN/InAlN Multiple Quantum Wells in Core-Shell Wire Structure for UV Emission. *ACS Photonics.* 2014, *Vol. 1*, 38−46.

(25) Ambacher, O.; Foutz, B.; Smart, J.; Shealy, J. R.; Weimann, N. G.; Chu, K.; Murphy, M.; Sierakowski, A. J.; Schaff, W. J.; Eastman, L. F.; et al. Elastic Properties of Zinc-Blende and Wurtzite AlN, GaN, and InN. *J. Appl. Phys.* 1997, *Vol.* 82, 2833−2839.

(26) Figge, S.; Kröncke, H.; Hommel, D.; Epelbaum, B. M. Temperature Dependence of the Thermal Expansion of AlN. *Appl. Phys. Lett.* 2009, *Vol. 94*, 101915.

(27) Koester, R.; Hwang, J. S.; Durand, C.; Le Si Dang, D.; Eymery, J. Self-Assembled Growth of Catalyst-Free GaN Wires by Metal-Organic Vapour Phase Epitaxy. *Nanotechnology.* 2010, *Vol. 21*, 015602.

(28) Tchoulfian, P.; Donatini, F.; Levy, F.; Amstatt, B.; Ferret, P.; Pernot, J. High Conductivity in Si-Doped GaN Wires. *Appl. Phys. Lett.* 2013, *Vol. 102*, 122116.

(29) Tchoulfian, P.; Donatini, F.; Levy, F.; Dussaigne, A.; Ferret, P.; Pernot, J. Direct Imaging

of P-n Junction in Core-Shell GaN Wires. *Nano Lett.* 2014, *Vol. 14*, 3491–3498.

(30) Kapoor, A.; Finot, S.; Grenier, V.; Robin, E.; Bougerol, C.; Bleuse, J.; Jacopin, G.; Eymery, J.; Durand, C. Role of Underlayer for Efficient Core-Shell InGaN QWs Grown on m-Plane GaN Wire Sidewalls. *ACS Appl. Mater. Interfaces.* 2020, *Vol. 12*, 19092–19101.

(31) Gilet, P.; Dussaigne, A.; Salomon, D.; Eymery, J.; Durand, C. Optoelectronic Device Comprising Three-Dimentional Semiconductors Elements, and Method for Manufacturing Said Device. US Pat. App.15/745,429, July 26, 2018.

(32) Rafaja, D.; Fischer, P.; Barchuk, M.; Motylenko, M.; Röder, C.; Besendörfer, S.; Meissner, E. X-Ray Diffraction Analysis and Modeling of the Depth Profile of Lattice Strains in AlGaN Stacks. *Thin Solid Films.* 2021, Vol. *732,* 138777.

(33) Follstaedt, D. M.; Lee, S. R.; Allerman, A. A.; Floro, J. A. Strain Relaxation in AlGaN Multilayer Structures by Inclined Dislocations. *J. Appl. Phys.* 2009, Vol. *105*, 083507.

(34) Bethoux, J. M.; Vennéguès, P.; Natali, F.; Feltin, E.; Tottereau, O.; Nataf, G.; De Mierry, P.; Semond, F. Growth of High Quality Crack-Free AlGaN Films on GaN Templates Using Plastic Relaxation through Buried Cracks. *J. Appl. Phys.* 2003, *Vol. 94*, 6499–6507.

(35) Einfeldt, S.; Dießelberg, M.; Heinke, H.; Hommel, D.; Rudloff, D.; Christen, J.; Davis, R. F. Strain in Cracked AlGaN Layers. *J. Appl. Phys.* 2002, *Vol. 92*, 118–123.

(36) Vashaei, Z.; Bayram, C.; Lavenus, P.; Razeghi, M. Photoluminescence Characteristics of Polar and Nonpolar AlGaN/GaN Superlattices. *Appl. Phys. Lett.* 2010, *Vol. 97*, 121918.

(37) Birner, S.; Hackenbuchner, S.; Sabathil, M.; Zandler, G.; Majewski, J. A.; Andlauer, T.; Zibold, T.; Morschl, R.; Trellakis, A.; Vogl, P. Modeling of Semiconductor Nanostructures with Nextnano3. *Acta Phys. Pol. A.* 2006, *Vol. 110*, 111–124.

(38) Kandaswamy, P. K.; Guillot, F.; Bellet-Amalric, E.; Monroy, E.; Nevou, L.; Tchernycheva, M.; Michon, A.; Julien, F. H.; Baumann, E.; Giorgetta, F. R.; *et al*. GaN/AlN Short-Period Superlattices for Intersubband Optoelectronics: A Systematic Study of Their Epitaxial Growth, Design, and Performance. *J. Appl. Phys.* 2008, *Vol. 104*, 093501.

# For Table of Contents Use Only

## Toward crack-free core-shell GaN/AlGaN quantum wells

Vincent Grenier [1,a)], Sylvain Finot[2], Bruno Gayral[1], Catherine Bougerol[2], Gwénolé Jacopin[2], Joël Eymery[3] and Christophe Durand[1]

[1] *Univ. Grenoble Alpes, CEA, IRIG, PHELIQS, NPSC, 38000 Grenoble, France*

[2] *Univ. Grenoble Alpes, CNRS, Grenoble INP, Institut Néel, 38000 Grenoble, France*

[3] *Univ. Grenoble Alpes, CEA, IRIG, MEM, NRS, 38000 Grenoble, France*

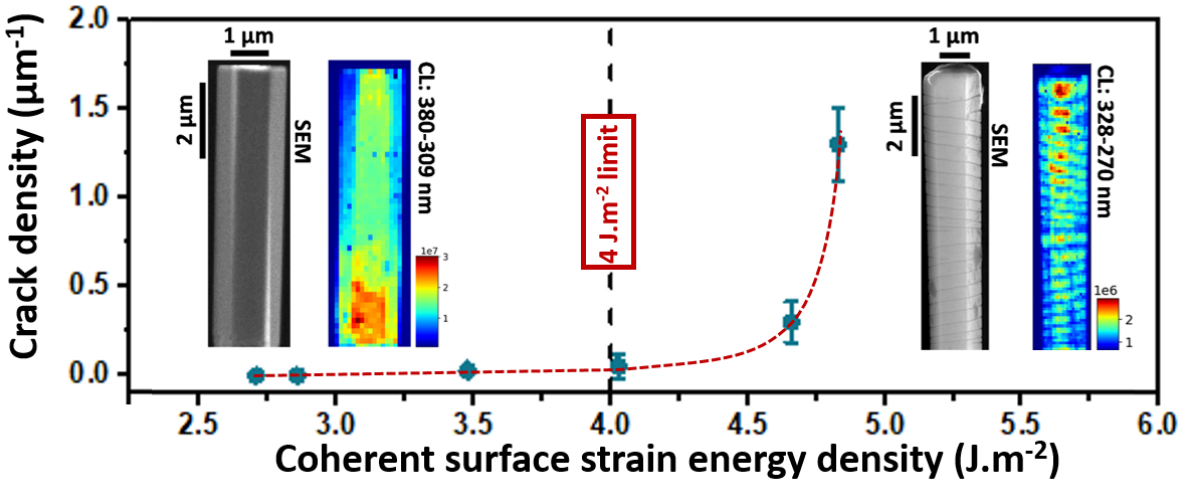


*TOC : Crack generation in core-shell GaN/ wires grown by MOVPE. Existence of energy threshold and impact on UV emission.*